ASPERA-3: Analyser of Space Plasmas and Energetic Neutral Atoms

R. Lundin[1], S. Barabash[1] and the ASPERA-3 team: M. Holmström[1], H. Andersson[1], M. Yamauchi[1], H. Nilsson[1], A. Grigorev, D. Winningham[2], R. Frahm[2], J.R. Sharber[2], J.-A. Sauvaud[3], A. Fedorov[3], E. Budnik[3], J.-J. Thocaven[3], K. Asamura[4], H. Hayakawa[4], A.J. Coates[5], Y. Soobiah[5] D.R. Linder[5], D.O. Kataria[5], C. Curtis[6], K.C. Hsieh[6], B.R. Sandel[6], M. Grande[7], M. Carter[7], D.H. Reading[7], H. Koskinen[8], E. Kallio[8], P. Riihela[8], T. Säles[8], J. Kozyra[9], N. Krupp[10], J. Woch[10], M. Fraenz[10], J. Luhmann[11] , D. Brain[11], S. McKenna-Lawler[12], R. Cerulli-Irelli[13], S. Orsini[13], M. Maggi[13], A. Milillo[13], E. Roelof[14], S. Livi[14], P. Brandt[14], P. Wurz[15], P. Bochsler[15] & A. Galli[15]

[1] *Swedish Institute of Space Physics, Box 812, S-98 128 Kiruna, Sweden*
[2] *Southwest Research Institute, San Antonio, TX 7228-0510, USA*
[3] *Centre d'Etude Spatiale des Rayonnements, BP-4346, F-31028 Toulouse, France*
[4] *Institute of Space and Astronautical Science, 3-1-1 Yoshinodai, Sagamichara, Japan*
[5] *Mullard Space Science Laboratory, University College London, Surrey RH5 6NT, UK*
[6] *University of Arizona, Tucson, AZ 85721, USA*
[7] *Rutherford Appleton Laboratory, Chilton, Didcot, Oxfordshire OX11 0QX, UK*
[8] *Finnish Meteorological Institute, Box 503, FIN-00101 Helsinki, Finland; and Department of Physical Sciences, PO Box 64, University of Helsinki, FIN-00014 Helsinki, Finland*
[9] *Space Physics Research Laboratory, University of Michigan, Ann Arbor, MI 48109-2143, USA*
[10] *Max-Planck-Institut für Sonnensystemforschung, D-37191 Katlenburg-Lindau, Germany*
[11] *Space Science Laboratory, University of California at Berkeley, Berkeley, CA 94720-7450, USA*
[12] *Space Technology Ltd, National University of Ireland, Maynooth, Co. Kildare, Ireland*
[13] *Istituto di Fisica dello Spazio Interplanetario, I-00133 Rome, Italy*
[14] *Applied Physics Laboratory, Johns Hopkins University, Laurel, MD 20723-6099, USA*
[15] *University of Bern, Physikalisches Institut, CH-3012 Bern, Switzerland*

The Analyser of Space Plasma and Energetic Neutral Atoms (ASPERA-3) on Mars Express (MEX) has now completed one martian year in orbit. The experiment has performed very well and has yielded many interesting findings about the interaction of the solar wind with the planet Mars. ASPERA-3 has revealed that solar wind plasma and accelerated ionospheric ions may be observed all the way down to the MEX pericentre (250–300 km) above the dayside planetary surface. This is quite deep in the ionosphere and atmosphere, implying strong solar wind plasma forcing. The low-altitude ion energisation and outflow near Mars is surprisingly similar to that over the strongly magnetised planet Earth – from narrow 'mono-energetic' ion beams to beams with a broad energy distribution. The distribution of the accelerated plasma suggests both a direct solar wind energy and momentum exchange, via for instance, waves produced by the shocked solar wind, and an indirect solar wind interaction inducing electric currents and fields in a magnetised plasma environment. In the latter case we also envisage parallel (to the magnetic field) electric currents and electric fields projected onto regions of crustal magnetisation in the nightside ionosphere of Mars.

Using a novel measurement technique for energetic neutral atoms (ENAs), ASPERA-3 is exploring a new dimension in the solar wind interaction with unmagnetised planets. Mars is 'shining' in energetic neutral atoms. Part of this is caused by reflections of inflowing hydrogen ENAs from the solar wind, but a large fraction is emitted via charge exchange when hot plasma, of solar wind and planetary wind origin, interacts with the upper atmosphere. In this chapter we briefly review three ENA phenomena related to Mars – ENA albedo, ENA jets and ENA occultation. We also discuss another, yet to be explained, source of ENAs in interplanetary space. This source is most likely related to the heliospheric boundaries, but other explanations should also be considered.

1. Introduction

Solar forcing has a strong impact on Earth-like planets, on a long-term as well as short-term basis. The solar electromagnetic radiation, from X-rays to infrared, provides the highest input power to the planetary environment; for Mars, with its elliptical orbit, the power varies between ~90 and 720 W m^{-2}. The corpuscular (particle flux) power from the solar wind is up to six orders of magnitude less than that. Yet, it is known that the solar wind plays an important, if not the major, role in the erosion of the martian atmosphere. The heating of the martian exosphere leads to a mass loss from Jeans (thermal) escape an order of magnitude less than nonthermal escape governed by the solar wind with an input power of just ~0.001 W m^{-2}. This demonstrates that physical processes matter more than sheer power for the escape of planetary volatiles.

Thermal (Jeans) escape from an atmosphere is determined from a Maxwellian (thermalised) particle distribution, the escape rate given by the temperature of the distribution at the exobase and the escape velocity of the object at the exobase. Theoretically, all particles within a Maxwellian distribution of particles having velocities above the escape velocity will be lost. *Nonthermal escape* may be defined as all other processes where the energisation and escape of particles are related to (microscopic) nonthermal processes. In our case we define nonthermal escape as the result of external plasma (solar wind) forcing. All other processes of catastrophic nature, such as impact erosion by objects infalling from space, are excluded. Nonthermal escape is not unrelated to thermal escape, because most nonthermal escape processes are based on photoionisation, i.e. ionisation of the neutral upper atmosphere. The electromagnetic radiation from the Sun also determines the scale height of the atmosphere, and correspondingly also the ionosphere and target area for e.g. solar wind forcing. However, we separate these two mechanisms mainly because of their differences with respect to solar forcing.

A good illustration of nonthermal escape is the plasma (ion) tail of a comet. The plasma tail is due mainly to the interaction of the solar wind with ionised cometary matter. Despite general differences between a comet and a weakly magnetised planet like Mars, there are many similarities. The main difference between these objects is gravity. Mars has much stronger gravity that binds volatile substances for billions of years before being significantly eroded away by the solar wind. The low gravity of comets means that their atmosphere builds up and expands while approaching the Sun, leading to rapid erosion by the solar wind. Insertion in an Earth-like orbit would in fact completely empty a kilometre-sized comet of volatiles in typically one million years.

The direct interaction between the solar wind and the martian atmosphere contrasts with the indirect interaction of the solar wind with Earth. The radial standoff distance from Earth is typically 70 000 km in the subsolar region, while it is less than 1000 km for Mars (Gringauz, 1981). While solar wind energy has only limited access to Earth's auroral region, it has access to essentially the entire dayside, and part of the nightside ionosphere and atmosphere of Mars. The rate of erosion of the ionospheric plasma is consequently lower for Earth than for Mars.

Phobos 2, launched in July 1988, was the first spacecraft that enabled a quantitative estimate of the volatile escape from Mars. Based on the energised outflow of H^+,

O^+, O_2^+ and CO_2^+ detected by the ASPERA experiment on Phobos 2 (Lundin et al., 1989), it was possible to estimate the volatile loss from Mars to ~1 kg s^{-1}. Assuming for simplicity that the outflow originates from CO_2 and not from water (oxygen and proton), we obtain a theoretical atmospheric lifetime of ~200 million years. However, as indicated by the ion escape data (e.g. Lundin et al., 1989; Norberg et al., 1993; Carlsson et al., 2005), the dominant ions are O^+, and O_2^+, indicating a preference for loss of water, with CO_2 molecules disappearing at a much slower rate even though the CO_2/H_2O content ratio in the atmosphere is about 1000. Dehydration therefore appears to be the most efficient process with regard to ion escape, to the extent that it may even dominate the escape of volatiles from arid planets like Mars.

In this chapter we report on results from the ASPERA-3 investigation after two years in orbit. Our purpose is not to review the entire volume of 24 papers already published, plus some 10 more that are in the process of being published, but rather to offer a flavour of some interesting findings by ASPERA-3. We present results from all sensors, covering important aspects of the scientific objectives of the ASPERA-3 investigation. We focus on two themes: the solar wind interaction and the ionospheric plasma escape – the planetary wind, and the energetic neutral particle environment of Mars.

2. The ASPERA-3 Investigation

2.1 Scientific Objectives

The scientific objectives of the ASPERA-3 experiment on Mars Express (Barabash et al., 2004) are to study the short- and long-term effects of the solar wind interaction with the martian atmosphere and ionosphere, by means of, first, remote sensing of energetic neutral atoms (ENAs), enabling us to:

- image the *global solar wind interaction* with the martian ionosphere and atmosphere;
- characterise quantitatively the *plasma interaction with the atmosphere*;
- determine the *morphology of the global plasma and neutral gas outflow at Mars*; and
- determine the net outflow of ENAs from Mars.

Second, by measuring *in situ* the hot plasma, it is possible to:

- investigate the transfer of energy, mass and momentum of the solar wind plasma to the martian ionosphere and upper atmosphere;
- determine the plasma acceleration/outflow from the martian ionosphere, part of the outflow charge-exchanging to ENAs;
- provide undisturbed solar wind parameters required for the interpretation of ENA images; and
- determine the rate of ionospheric plasma outflow, the planetary wind.

2.2 The ASPERA-3 Instrument

The ASPERA-3 instrument comprises four sensors, two ENA sensors, and electron and ion spectrometers. The two ENA sensors are optimised for some of the scientific objectives while at the same time complementing each other. This approach provides the necessary redundancy as well as the independent cross-checks that are necessary for such ‘first-ever’ measurements. The charged particle sensors not only provide characterisation of the local plasma environment but they also support ENA measurements in terms of charged particle background and inter-calibrations. ASPERA-3 consists of four experiments:

The *Neutral Particle Imager (NPI)* provides measurements of the integral ENA flux with no mass and energy resolution but with 5° × 11° angular resolution. The intrinsic field of view is 9° × 344°. The sensor utilises a graphite surface to suppress the UV background. ENAs incident on the surface at a grazing angle of 20° are

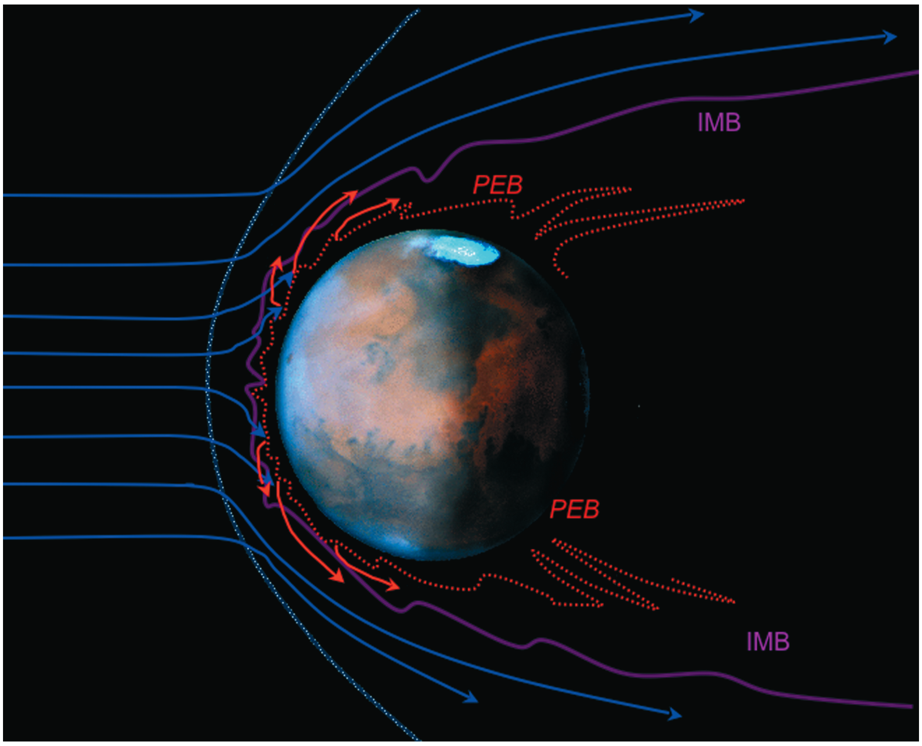

Fig. 1. The comet-like solar wind interaction with Mars, showing some of the characteristic features observed: the deeply corrugated penetration of the solar wind into the dayside atmosphere; an induced magnetosphere boundary (IMB) with the solar wind plasma outside and planetary plasma (the planetary wind) inside; and the photoelectron boundary (PEB) dominated by a cold ionospheric plasma.

reflected and/or cause ion sputtering. A micro-channel plate (MCP) stack detects the reflected particles and sputtered fragments with a discrete anode.

The *Neutral Particle Detector (NPD)* provides measurements of the ENA differential flux over the energy range 100 eV–10 keV, resolving H and O with a coarse 5° × 30° angular resolution. The sensor consists of two identical detectors, each with a 9° × 90° intrinsic field of view. The measurement technique is based on a principle similar to that of the NPI, but using in addition a time-of-flight technique that gives the ENA velocity. The pulse–height distribution analysis of the STOP signals is used to provide a rough determination of the ENA mass.

The *Electron Spectrometer (ELS)* provides electron measurements in the energy range 0.01–20 keV. The intrinsic field of view is 10° × 360°. The 360° aperture is divided into 16 sectors. The sensor is a standard top-hat electrostatic analyser in a very compact design.

The *Ion Mass Analyser (IMA)* provides ion measurements in the energy range 0.01–30 keV/Q for the main ion components: H^+, He^{++}, He^+, O^+, O_2^+ and CO_2^+. The IMA has a 4.6° × 360° field of view. Electrostatic sweeping provides elevation (±45°) coverage, thus giving coverage of half the unit sphere.

3. The Solar Wind Interaction and the Planetary Wind

The new results obtained from the ASPERA-3 ion and electron analysers have considerably improved our understanding of the solar wind interaction with Mars. Lundin et al. (2004), for instance, noted that the solar wind penetrates deep into the dayside atmosphere, accelerating ions to high energies even at very low altitudes. This implies that the entire dayside atmosphere of Mars is under more intense solar wind forcing than previously believed. The data also suggest that the forcing leads to a highly corrugated contact surface between the ionosphere and the solar wind. This may in part be due to spatial/temporal irregularities in the solar wind, but it may also be related to the patchy crustal magnetisations at Mars (Acuña et al., 1999) and their associated ‘cusps’ (Krymskii et al., 2002). Ion data from the flank and tail of Mars suggest many similarities between Mars and comets, i.e. the accelerated outflowing

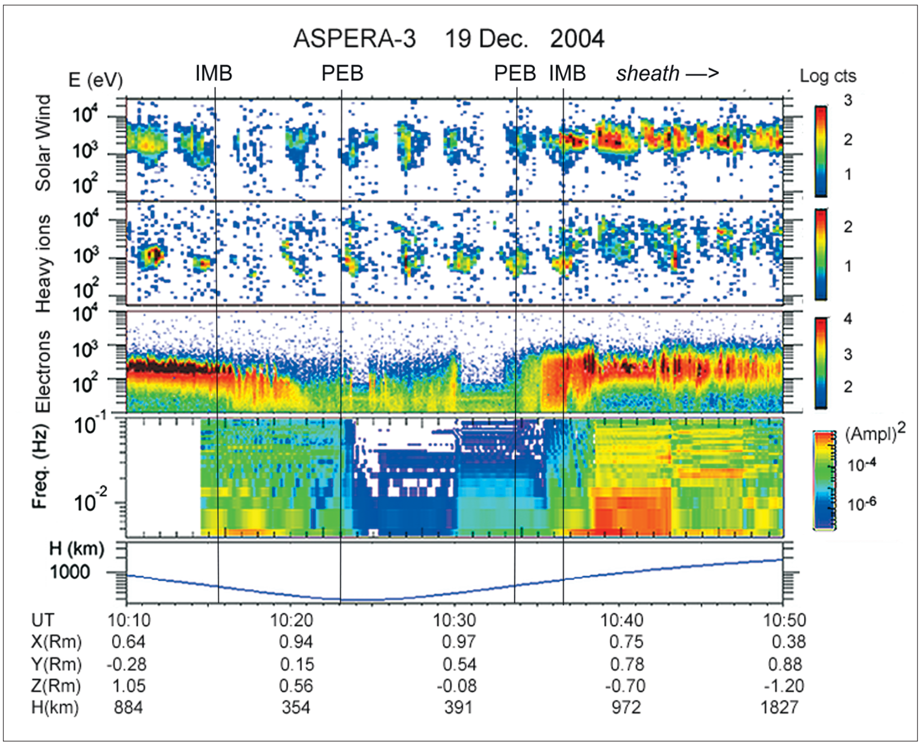

Fig. 2. Energy–time spectrogram of ions and electrons (top three panels) and electron frequency spectra (bottom panel) from a dayside pericentre (297 km) pass near local noon, 19 December 2004, illustrating the presence of the solar wind and energised heavy ions down to the spacecraft pericentre. The IMB and PEB boundaries are indicated (after Lundin et al., 2006b).

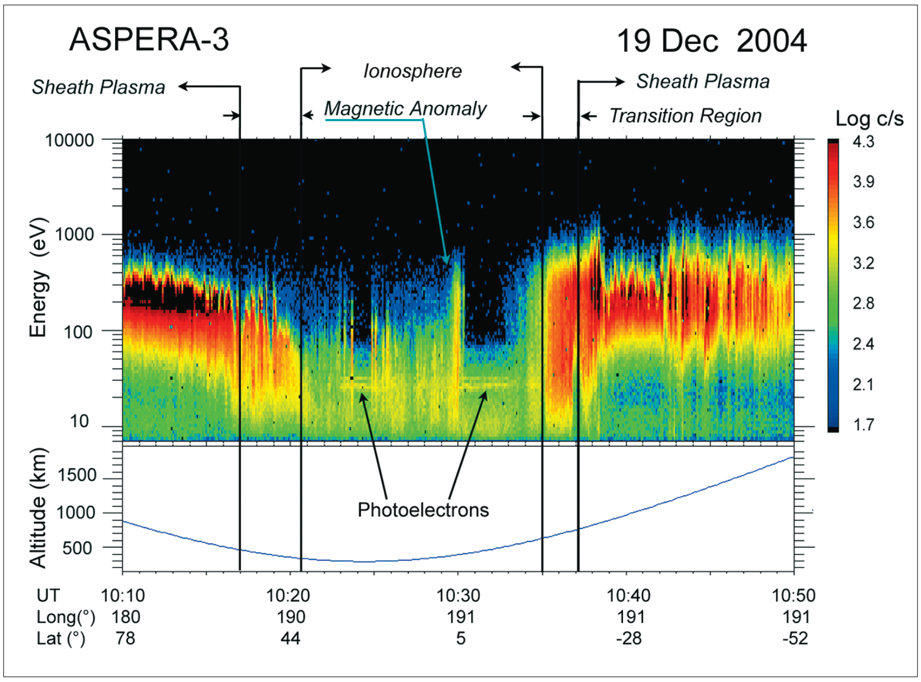

Fig. 3. Energy–time spectrogram of electrons for a periapsis pass into the dayside ionosphere, showing some the characteristic features, such as the photoelectron lines, the signature of an electron anomaly, and the transition into the sheath (PEB).

ionospheric plasma is quite structured, and the bulk of the flow follows the external solar wind flow in the anti-sunward direction (e.g. Dubinin et al., 2006).

The morphology of the ionospheric plasma outflow from Mars is shown in Fig. 1. Most of the accelerated ionospheric plasma outflow is contained inside the induced magnetosphere boundary (IMB), while the cold ionospheric plasma is contained inside the photoelectron boundary (PEB). Figure 2 shows ion and electron energy–time spectra for a MEX dayside pericentre traverse, and illustrates how the IMB and PEB

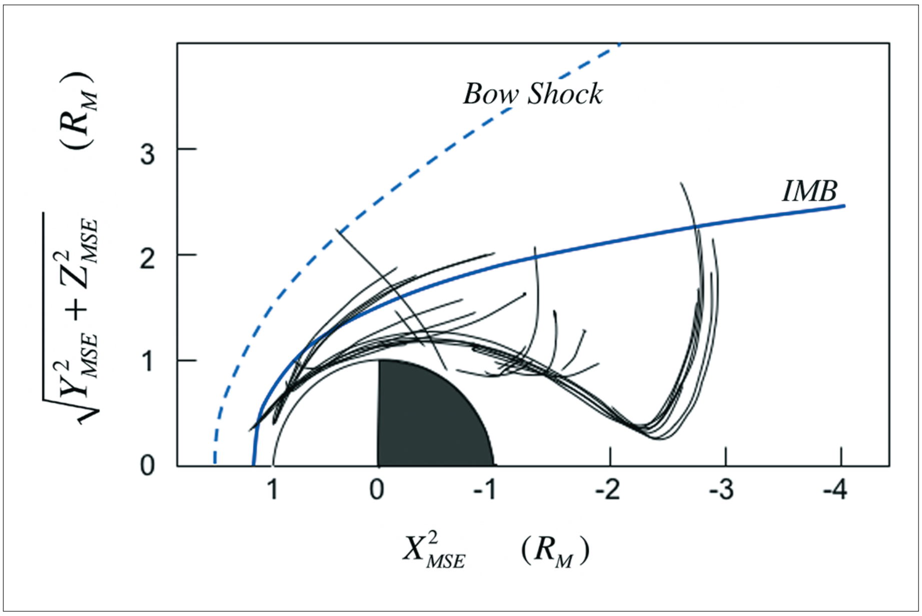

Fig. 4. Morphology of the planetary ion acceleration and outflow. MEX trajectory traces with observations of ion acceleration and outflow are depicted using a cylindrical coordinate system. IMB marks the average induced magnetosphere boundary.

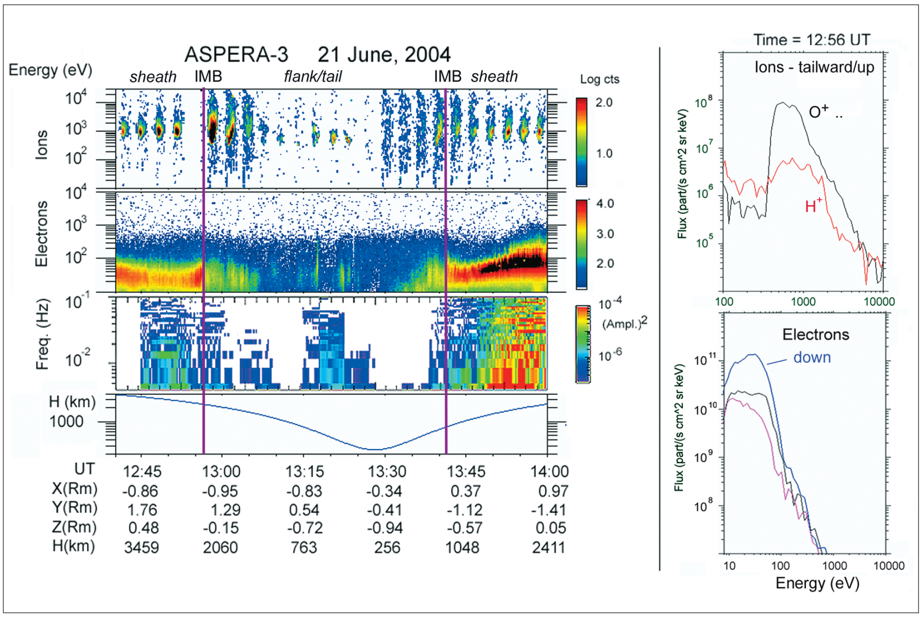

Fig. 5. IMI and ELS data from a MEX pericentre pass on June 21 2004. Right panel, top: data (counts) of tailward-moving planetary ions (*m*/*q*=16–44 amu). Left panel, centre: downward-moving electron energy spectra (counts) and the frequency spectra of electrons, respectively. The ion and electron flux spectra in the right panel were taken at 12:56 UT (Lundin et al., 2006b).

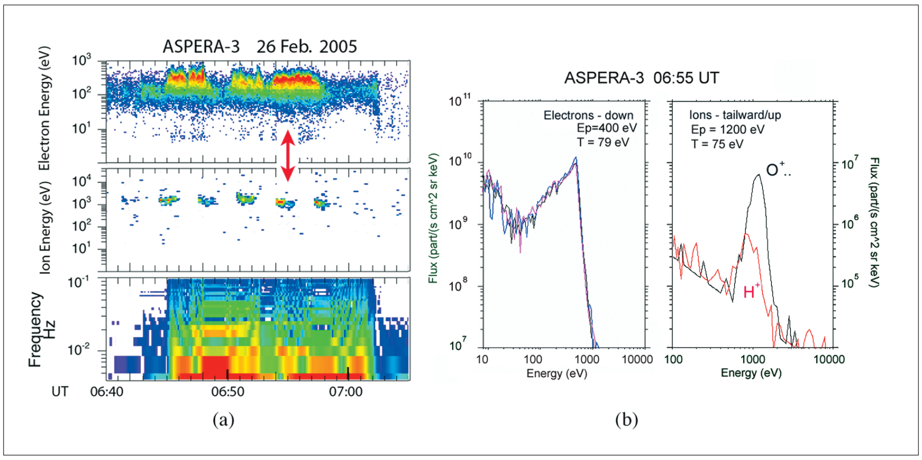

Fig 6. (a) Energy–time spectrogram for electrons and ions showing plasma acceleration in the deep nightside. (b) Energy spectra of oppositely accelerated electron and ion fluxes in the central tail, taken at 06:55 UT (Lundin et al., 2006b).

were identified using ASPERA-3 data. The figure also demonstrates that solar wind ions protrude all the way down to pericentre (here 300 km). At the same time we observe energisation of planetary (heavy) ions.

The Electron Spectrometer (ELS) has demonstrated a unique capability to resolve the fine structure in electron spectra, such as the CO_2 photoelectron peaks (Frahm et al., 2006). In Fig. 3, as well as the photoelectron lines in the 'cold' ionospheric plasma, we can also observe the 'magnetic anomaly' features first discovered by the Mars Global Surveyor (MGS; Acuña et al., 1999; Mitchell et al., 2001). The magnetic anomalies, caused by crustal magnetisations at Mars, are of particular interest for the solar–planetary relationship. The high energy and time resolution of the ELS is a very important asset for understanding the plasma environment of Mars.

The energisation and escape of planetary ionospheric ions were discussed in detail in several papers in a special issue of *Icarus* (vol. 182(2)) in 2006. We present here an extract of the energisation and outflow from a study covering the dayside, flank and tail of Mars (Lundin et al., 2006b). Fig. 4 illustrates the locations of observed energisation and outflow; note that most of the observations are made within the average magnetic pile-up boundary (MPB)/IMB boundary. An example of a dayside/flank ion energisation of heavy ions associated with what was termed 'streaming' electrons of magnetosheath origin is shown in Fig. 5. The outflows of H^+ and O^+ are substantially heated, with beam temperatures reaching several hundred eV. This should be compared with ionospheric ion temperatures of typically <1 eV. Thus, heating, possibly by waves (Espley et al., 2005; Winningham et al., 2006), is an important ionospheric plasma energisation and escape process in the dayside and flank of Mars.

Further downstream, inside the tail cavity of Mars, the ion energisation characteristics are quite different from those in the dayside and flank. Observations from Phobos-2 suggested accelerated narrow/cold beams inside a 'plasma sheet' (Lundin et al., 1992). Dubinin et al. (1993) considered the ion acceleration to be due to the solar wind motional emf. ASPERA-3 measurements inside the tail cavity, as shown in Fig. 6, suggested slightly different, more Earth-like, plasma acceleration processes. The narrowly peaked ion and electron spectra and the 'inverted V'-like energy–time spectra, as observed in Fig. 6, suggested plasma acceleration by magnetic field aligned electric fields. Mars lacks a strong intrinsic magnetic dynamo, but has instead confined magnetised regions dispersed in the crust (Acuña et al., 1999). The multi-pole magnetisation pattern on Mars implies that magnetic cusps are formed (Krymskii et al., 2002) that extend into space. In analogy with Earth, it was therefore believed that magnetic field-aligned plasma acceleration, and a discrete aurora, would occur above Mars. With Mars Express we have now confirmed the characteristic plasma acceleration and auroral emissions in the nightside of Mars (Bertaux et al., 2005; Lundin et al., 2006a). Mars Global Surveyor (MGS) has also confirmed the existence of field-aligned electric currents associated with the auroral electron acceleration above Mars (Brain et al., 2006). Figure 7 (after Lundin et al., 2006a) shows a diagrammatic representation of the field acceleration of ions and electrons, constituting what is known from Earth as the 'auroral acceleration process'.

The composition of the ion outflow from Mars reflects the depth of solar forcing in the martian ionosphere. A study of the ion outflow composition by Carlsson et al. (2006) indicated almost equal amounts of O^+ and O_2^+, with CO_2^+ contributing 10% to the outflow. More comprehensive statistics may show that the O_2^+ abundance is higher. Figure 8 shows ASPERA-3 ion composition data (Lundin et al., 2006b) combined with an ionospheric density and ion composition profile determined by the Viking-1 lander (Hansson et al., 1977). Note that the accelerated ion composition of the outflow in 2004 was similar to the ionospheric composition in the altitude range 230–250 km as measured by Viking-1 in 1974. These two observations were made 20 years apart, but both were made during the declining phase of solar activity. The general conclusion from this, based on the composition of the ion outflow, is that solar forcing extends down to quite low altitudes in the ionosphere of Mars, where molecular ionospheric ions can also be accelerated.

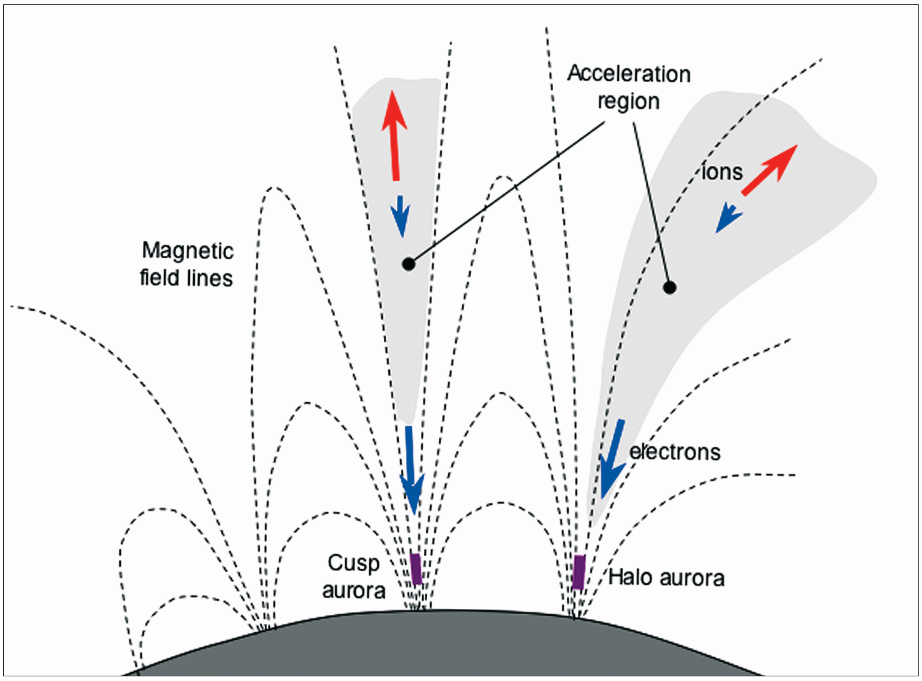

Fig. 7. Auroral plasma acceleration above the magnetic anomalies at Mars. A cusp/cleft aurora is expected to occur between adjacent anomalies, and a halo aurora to circumscribe the large-scale region of crustal magnetisation (Lundin et al., 2006a).

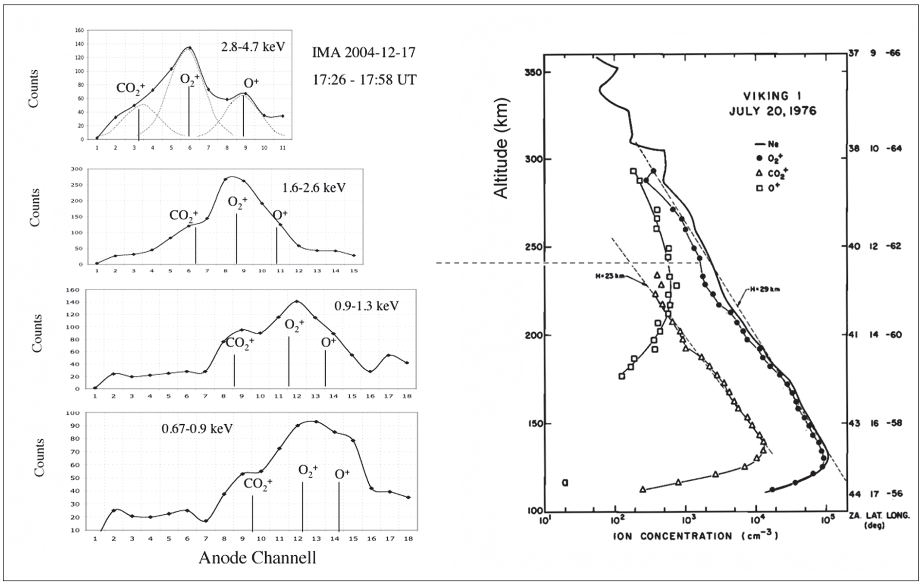

Fig. 8. Left: Ion mass spectra illustrating the composition of the ionospheric outflow from Mars, with O_2^+ most abundant, followed by O^+ and CO_2^+ (Lundin et al., 2006b). The composition is similar to that observed by Viking 1 at an altitude of about 240 km (figure from Hanson et al., 1977).

4. The Energetic Neutral Environment of Mars

From simulations of the martian ENA environment (e.g. Kallio et al., 1997; Holmström et al., 2002) it was expected that the ENA environment would encompass many interesting aspects of the solar wind interaction with Mars. The data have confirmed some of our simulation results, but they have also revealed many novel characteristics and new aspects. The latter is no surprise, considering how new and unexplored the ENA environment of Mars is. In the following we present some new discoveries by ASPERA-3 on Mars Express. The discoveries are all at such an early stage that it will take some time before their implications can be fully revealed. Four topics are briefly described here: (1) solar wind ENA albedo; (2) dayside ENA jets; (3) ENA occultation; and (4) an unknown source of interplanetary ENAs. Figure 9 illustrates the martian ENA environment based on ASPERA-3 observations (topics 1–3).

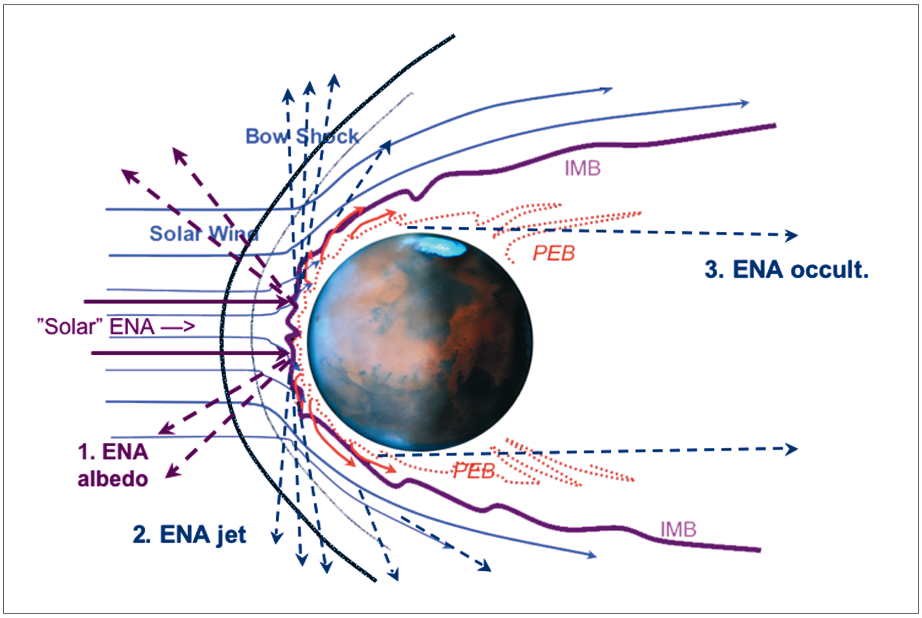

Fig. 9. The three main regions of ENA generation at Mars: 1, solar wind ENA albedo; 2, ENA 'jets'; and 3, tail/cavity ENA occultation.

4.1 Solar Wind ENA Albedo

The solar wind has an energetic neutral hydrogen component originating from two sources, the solar 'atmosphere/exosphere', and via charge exchange with interplanetary and interstellar neutrals. Energetic neutral hydrogen is always generated via charge exchange – a process whereby an incident ion (singly charged) picks up an electron from a (cold) neutral atom. The electron pick-up leads to a fast neutral atom and an ionised target atom. Charge exchange is therefore an ionisation as well as a conversion process – converting fast ions to fast neutrals. The results of solar wind ions impacting into the upper atmosphere of Mars are to contribute to the ionisation of the dayside atmosphere, as well as to produce a 'radiating' flow of ENAs. The flow of ENAs produced by ion collision with the martian atmosphere therefore adds to the incident solar wind ENA flow, both having the same energy as the solar wind because the energy loss in the charge exchange process is negligible. An interesting aspect of the ENA albedo is that it mimics the ion precipitation at Mars, enabling mapping of the dayside particle precipitatBackscattered ENAs are produced when the incident ENAs reach the exobase of Mars, experience elastic and inelastic collisions (Kallio and Barabash, 2000), and some of them are scattered back into space. Kallio and Barabash (2001) used a three-dimensional Monte Carlo model to investigate backscattered ENAs. They found a backscattering ratio of 0.58, the average energy of backscattered ENAs being ~60% of that of the incident ENAs.

Using the NPD instrument, Futaana et al. (2006a) measured backscattered ENAs from the martian upper atmosphere. This was the first observation of backscattered ENAs from the upper atmosphere of an unmagnetised planet. Figure 10 shows an example of such an observation. The left panel gives a 3D geometry of the MEX orbit and the NPD field of view (FOV) at 19:50 UT and 19:55 UT on 27 February 2004 in the Mars Solar Orbital (MSO) coordinate system. The white line represents the Mars Express trajectory, and the solid angles correspond to the NPD-2 FOVs. The right panels in Fig. 10 display NPD-2 time-of-flight (TOF) spectra integrated over the 5 min observation time for each direction. The dashed lines indicate the background count levels in each direction as defined by the low-energy channel. The TOF distribution has a broad spectrum at 150–500 ns (0.2–2.3 keV/amu), with a sharp peak embedded at 150–300 ns (0.6–2.3 keV/amu). We note here that the shocked solar wind protons detected by IMA during inbound into the sheath had energies of ~2 keV. This result

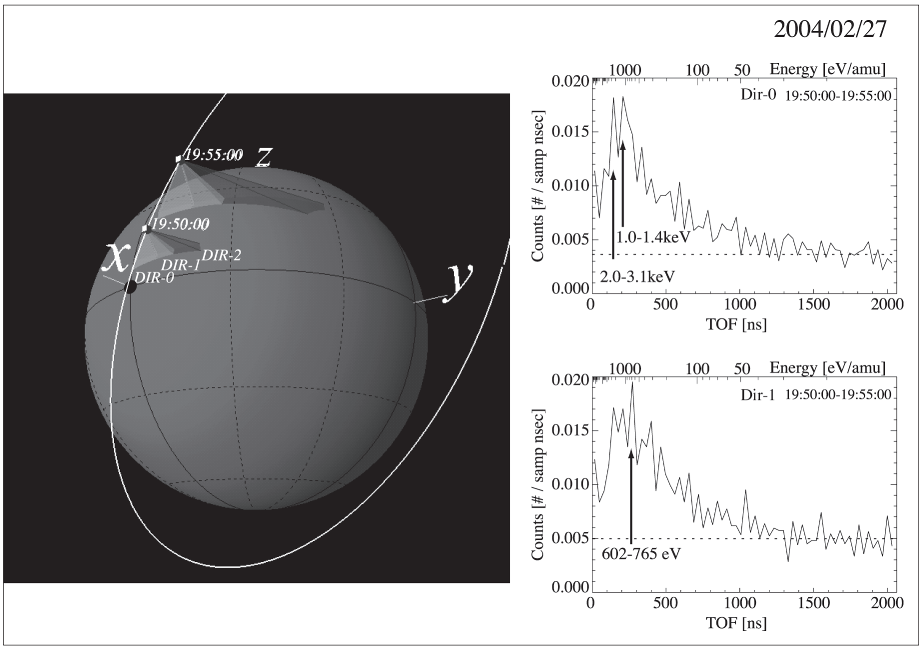

Fig. 10. Observations of backscattered ENAs (from Futaana et al., 2006b). Left panel: the MEX orbit and field of view of the NPD measurements. Right panels: TOF spectra for two directions integrated over the 5 min observation period.

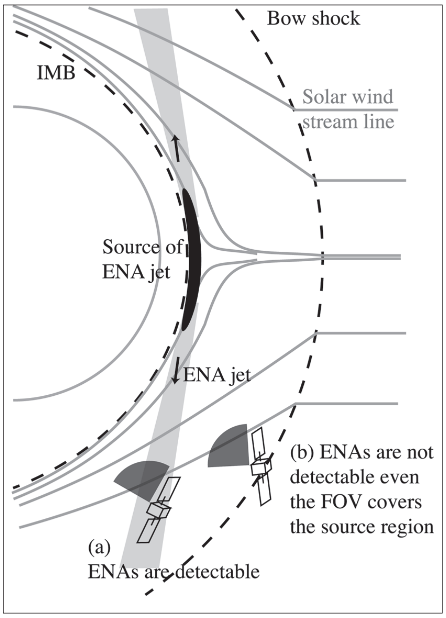

Fig. 11. Geometry of the subsolar ENA jet. The subsolar jet can be detected when the sensor is within it (case a). As soon as the spacecraft leaves the jet (case b) the ENAs cannot be detected even though the instrument FOV covers the source region (Futaana et al., 2006b).

is consistent with the ENAs originating from the solar wind interaction with Mars. Futaana et al. (2006a) inferred on basis of their observations a global backscattered ENA emission of ~10^7 cm^{-2} s^{-1}.

4.2 Dayside ENA Jets

The NPD and NPI sensors also detected a substantial flux of ENAs in the azimuthal direction (Gunell et al., 2006; Futaana et al., 2006b). They reported ENA signals coming from the dayside IMB–magnetosheath interface. By comparing the NPI data and an ENA generation model in the shocked solar wind, Kallio et al. (1997) concluded that they are the ENAs of shocked solar wind origin. On the other hand, Futaana et al. (2006b) measured the ENA flux emitted from the subsolar region using the NPD instrument, and named the outflow subsolar ENA jets, because the flux emission is highly directional from the subsolar region. Subsolar ENA jets may originate from two sources:

— Shocked solar wind protons charge-exchanging with planetary neutral atoms (Holmström et al., 2002) – the shocked solar wind is highly deflected in the subsolar region, and the velocity vector of the shocked solar wind flow points towards the azimuthal direction. When converted to ENAs, they form a subsolar ENA jet.
— Accelerated protons originating from hydrogen atoms in the martian upper atmosphere – the acceleration takes place in the exosphere by the solar wind interaction. The accelerated protons may subsequently charge-exchange back to ENAs (Lichtenegger et al., 2002).

In both cases, jets may be produced near local noon, in a region subject to head-on solar wind forcing. An opportunity to reveal in more detail the geometry and the cause of the ENA jets came during the passage of an interplanetary shock that displaced the ENA source region (Futaana et al., 2006c). During this event the NPD data exhibited an extremely high-flux ENA jet. The observed flux was approximately five times higher than typical fluxes, and decreased abruptly in a very short time, less than 10 s, when the spacecraft crossed an outer boundary of the ENA jet. The generation region of the subsolar ENA jet was pushed towards the planet by the interplanetary shock, as shown in Fig. 11. Mars Express subsequently went into and out of the ENA jet region

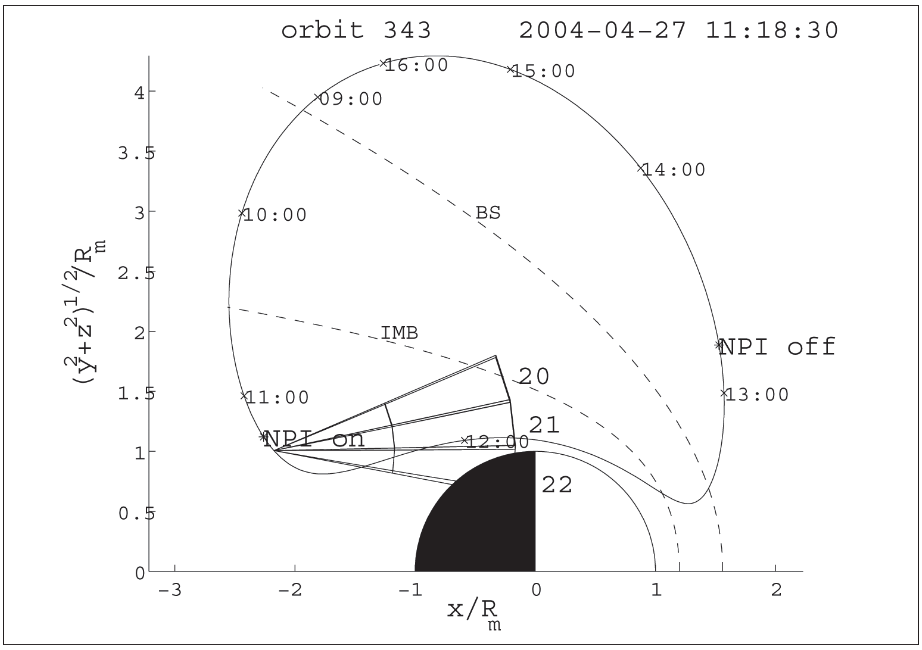

Fig. 12. A view of the orbit geometry with the field of view of NPI sectors 20–22 at 11:18:30 UT during orbit 343, 27 April 2004. The plot is in cylindrical coordinates (see text). UT hours are included in the plot. Distances are in Mars radii (R_m = 3397 km). The area between the bow shock (BS) and the induced magnetosphere boundary (IMB) is referred to as the magnetosheath (Brinkfeldt et al., 2006).

in a quasi-periodic fashion, suggesting a global 'vibration' induced by the external interplanetary shock pulse.

4.3 ENA Occultation

ENA occultation measurements were carried out when the ENA (IMI) imager on MEX moved into the Mars eclipse (Brinkfeldt et al., 2006). In the course of this movement the solar wind ions charge-exchange with the extended Mars exosphere and produce ENAs that can spread into the eclipse of Mars due to the ions' thermal spread. The IMI measurements showed a persistent signal from the solar direction for several minutes as the spacecraft moved into the eclipse. The geometry of the occultation experiment is shown in Fig. 12, which also illustrates how the data from three NPI sectors were analysed. The UV background in the data was carefully analysed, and the photon illumination of the spacecraft was inferred from the presence of photoelectrons in the ELS electron data. The upper panel of Fig. 13 shows IMI and ELS data during one occultation event; the spacecraft motion into the eclipse is clearly evident from the drop in the UV background in IMI and a corresponding drop in the number of photoelectrons. The remaining NPI signal in eclipse originates from the thermal spread of solar wind charge-exchanged ENAs. The lack of correlation between electron and NPI data in eclipse, as shown in the bottom panel in Fig. 13, indicates that ENAs dominate the NPI signal.

The above measurements agree with simulations and a theoretical analysis by Kallio et al. (2006) of an ENA beam propagating through the atmosphere near the therminator of Mars. The measurements are considered a precursor to a new technique, called *ENA sounding,* for measuring the properties of the solar wind and planetary exosphere by means of energetic neutral particles.

4.4 An Unknown Source of Interplanetary ENAs

We noted above that ENAs are generated at the Sun, in interplanetary space (charge exchange with interplanetary and interstellar neutrals), and near planets (charge exchange with a planetary atmosphere). In principle, ENAs are generated whenever hot plasma interacts with a neutral gas. ENAs may subsequently 'radiate' away like photons, affected only by gravity (marginally) and particle collisions. At sufficiently

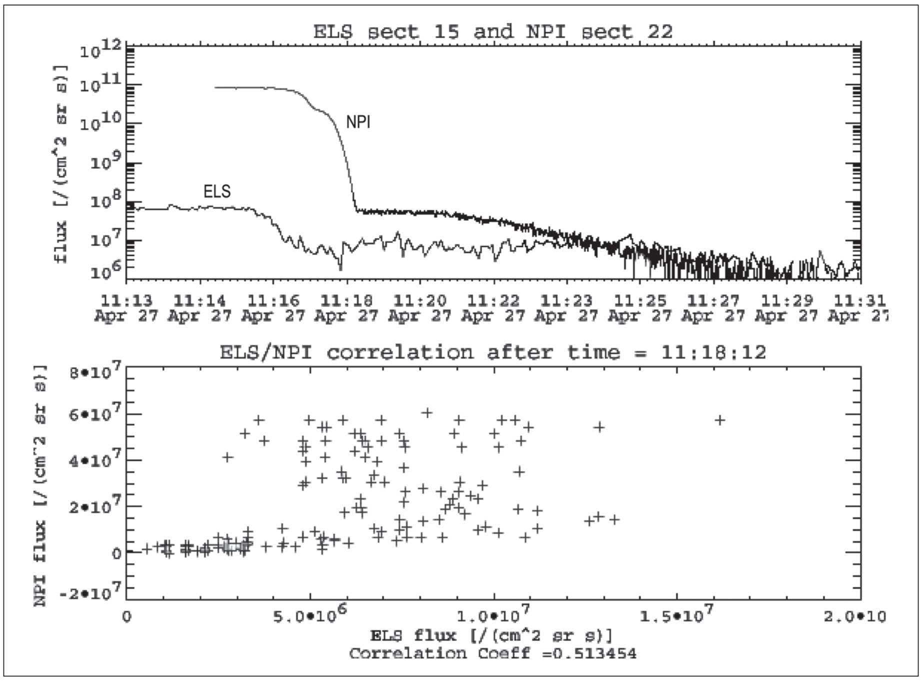

Fig. 13. Top panel: comparison of particle fluxes measured by NPI and ELS when entering eclipse. The ELS flux is integrated between 5 and 10 eV, and is a measure of photoelectron production on the spacecraft surface. It can thus give an indication of the UV background. Lower panel: the normalised NPI flux versus the normalised ELS flux. No correlation is observed (Brinkfeldt et al., 2006).

high velocities the ENAs may travel unperturbed for very long distances. ENA imaging, a concept that originates from Roelof et al. (1985), constitutes a means to study remotely hot plasma processes whenever hot plasma interacts with a neutral gas. The technique has evolved substantially since then, and has been utilised in missions to Earth's magnetosphere, such as Astrid 1 (Barabash et al., 1997) and Image (Burch, 2000), and now also on Mars, Venus and Titan (e.g. Mitchell et al., 2005).

The concept of plasma–neutral interaction has indeed much wider applications, and has led to speculation about its astrophysical implications. A more 'modest' speculation is the generation of heliospheric ENAs. Heliospheric ENAs are expected to be predominantly hydrogen neutrals produced on the far side of the termination shock in the inner heliosheath, where the solar wind slows down to subsonic speed. Heliospheric ENAs are produced by charge exchange between solar wind protons and interstellar neutrals, resulting in a detectable flux of inward-moving ENAs from the inner heliosheath (e.g. Gruntman et al., 2001). Imaging these ENAs and their energy spectra may help our understanding of the interaction of the heliosphere with the local interstellar environment.

Previous observations indicated the existence of energetic (keV) interplanetary neutrals (e.g. Collier et al., 2004). The NPD and NPI instruments were used to confirm and analyse the properties of such interplanetary ENA sources. An immediate problem is to distinguish between interplanetary neutrals and other (e.g. planetary) ENA sources. The first, and best, opportunity to study such sources occurred during the cruise phase. Barabash et al. (2004) reported the first data on keV neutrals that suggested a heliospheric or possibly exterior/interstellar origin. This was followed by studies combining cruise data and data in orbit around Mars by Holmström et al. (2006) and Galli et al. (2006).

Holmström et al. (2006) used NPI to observe ENA and UV fluxes in the shadow of Mars in 2004 and 2005. They were able to identify one signal that shifted position between those years, indicating that there are ENAs in this signal that are not related to the Mars–solar wind interaction. In addition, ENAs are seen in the eclipse that do emanate from the Mars–solar wind interaction, judging from the direction from which they came (near the limb of Mars). Figure 14 shows the evolution of the galactic plane

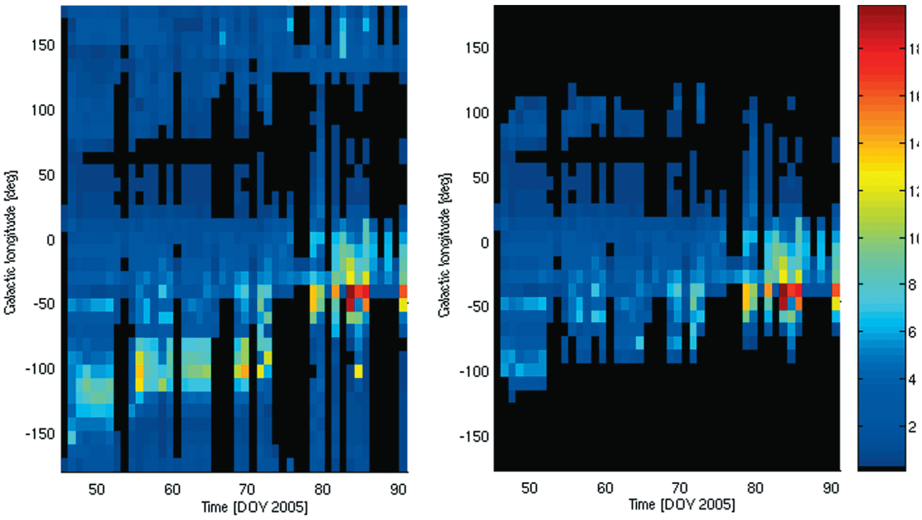

Fig. 14. Evolution of the galactic plane signal measured by NPI during 2005 (galactic coordinates). Right: the signal with all observations in the hemisphere of directions centred at Mars removed (Holmström et al., 2006)

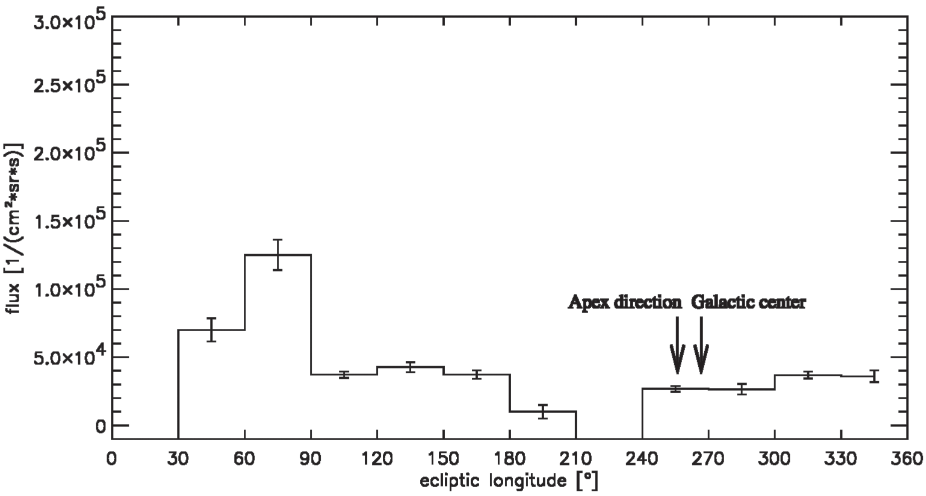

Fig. 15. Integral ENA flux versus direction of origin. The plot shows all measurements whose spectral shape fits the class described in section 4.4. The arrows at 255° and 267° ecliptic longitude denote the arrival direction of the interstellar neutral flow and the direction toward the galactic centre (Galli et al., 2006).

signal over time; we see a clear change in the signal at around –45° longitude. This change is present even if we look only at counts from the hemisphere away from Mars, excluding a Mars-related source (right).

Galli et al. (2006) used the NPD sensors to measure the energetic neutral hydrogen over a time range of 10 months when Mars was well out of the field of view. Figure 15 shows a typical example of an energy spectrum of non-planetary origin, reconstructed from NPD-2 data measured on 10 July 2003 during the cruise phase. A two-composite power law characterises the energy spectra with a moderate decrease at low energies. The break occurs close to 0.8 keV, with a steeper slope towards higher energies.

Figure 16 shows variations in the integral flux with ecliptic longitude. The Sun is moving relative to the local interstellar medium towards 255° at about 25 km s^{-1}. This results in a stream of low-energetic hydrogen and helium neutrals flowing from this direction towards the Sun (Witte, 2004; Lallement et al., 2005). The ENA signal measured by ASPERA-3, in contrast, seems to increase in integral flux between 30° and 90°, around the anti-apex direction, with a low-signal zone extending from 180° to 300°.

The source of the ENA signal observed by NPD as well as NPI is yet to be identified. There has to be a mechanism that produces neutral hydrogen fluxes in the order of 10^4–10^5 cm^{-2} sr^{-1} s^{-1}, with velocities of around 400 km s^{-1}. These velocities are an order of magnitude higher than the relative motion of the Sun through the local

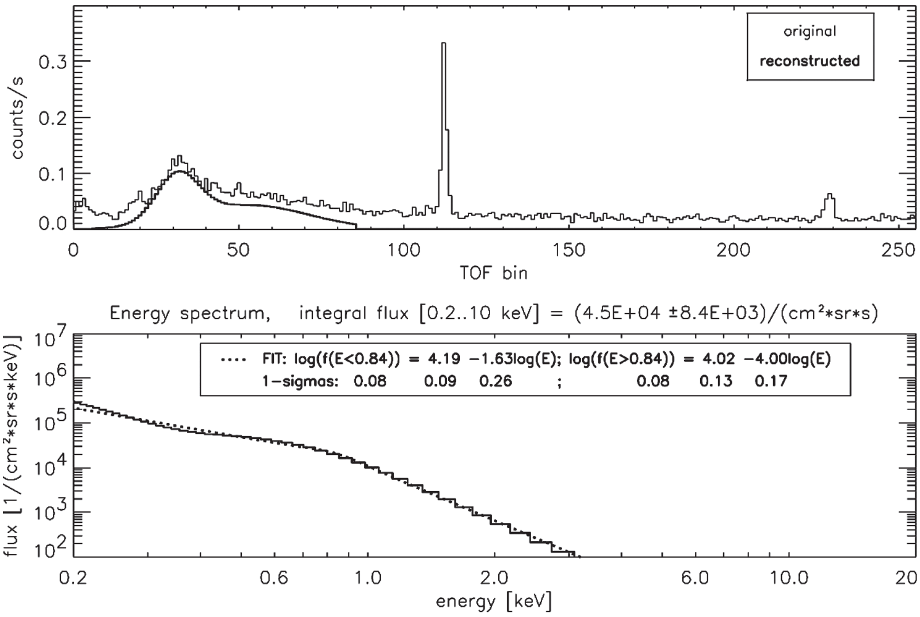

Fig. 16. Typical example of a non-planetary ENA signal (TOF, top panel) and derived flux energy spectrum, measured during the cruise phase (Galli et al., 2006).

interstellar cloud. The direction of highest fluxes of ENAs lies between 90° to 180° away from the direction of the interstellar neutral flow (Witte et al., 2004) and from the galactic centre.

5. Conclusions

ASPERA-3 has made a number of interesting new findings, most of them on the solar wind interaction with Mars, its ionosphere and atmosphere, but one of them related to the generation of ENAs in interplanetary space. These findings and their related consequences can be summarised as follows:

— The solar wind plasma may penetrate deep into the dayside ionosphere and atmosphere, 250–300 km, leading to strong solar wind forcing and the acceleration and outflow of planetary ions.
— Despite the lack of a strong intrinsic magnetic field, the low-altitude ion energisation and outflow from Mars are surprisingly similar to the ion energisation and outflow over Earth – from narrow ‘mono-energetic’ ion beams to beams with a broad energy distribution.
— The distribution of the planetary wind ions suggests two major acceleration processes: (a) direct solar wind energy and momentum exchange, via ion pickup and/or waves produced by the shocked solar wind, and (b) by ‘auroral plasma’ acceleration processes such as field-aligned electric fields in magnetic ‘cusps’ over nightside crustal magnetisation regions.
— Observations of plasma acceleration, ions upward and electrons downward, in confined cusp-like regions near local midnight, confirm the existence of an ‘equatorial aurora’ at Mars.

The ASPERA-3 ENA instruments have also made it possible to study completely new aspects of the solar wind interaction with an unmagnetised planet. Mars is ‘shining’ in energetic neutral atoms as a result of the solar wind interaction. Four aspects of the ENA emissions have been discussed:

— The backscattered/albedo of ENAs is caused in part by a reflection of inflowing hydrogen ENAs from the solar wind, but also via charge exchange when hot

plasma, of solar wind and planetary wind origin, interacts with the upper atmosphere.
- Subsolar ENA jets may originate from either shocked solar wind protons charge-exchanging with planetary neutral atoms, or accelerated protons originating from hydrogen atoms in the martian upper atmosphere.
- ENA occultation, representing a new technique called *ENA sounding,* can be used to measure solar wind and planetary exosphere properties by means of energetic neutral particles passing through the upper atmosphere/exosphere.
- Interplanetary/interstellar ENAs in the keV range, a completely new source of ENAs, are possibly generated in the heliosphere outside the termination shock. This observation introduces a new aspect of stellar objects in Universe, the possibility of these objects emitting, 'shining', substantial flows of energetic neutral atoms. This 'ENA shine' clearly must have an impact on astrophysics, and on how we conceive stellar objects in general and stellar spheres in particular.

In conclusion, we can now state that after two Earth-years in orbit around Mars, ASPERA-3 has been a great success. Since completion of this review, 22 papers based on ASPERA-3 data have been published in journals such as *Science*, *Icarus*, *Planetary and Space Sciences* and the *Astrophysical Journal*, and many more are pending. In view of the lead time involved, the number of publications after two years of data taking can be considered outstandingly high. ASPERA-3 has been a major success for its investigators, as well as for ESA and the Mars Express project.

Acknowledgements

The ASPERA-3 experiment on Mars Express is a joint effort involving 15 laboratories in 10 countries, all supported by their national agencies. We thank all of these agencies, as well as the various departments/institutes that are hosting these efforts. We wish to acknowledge in particular the Swedish National Space Board for its support for the main PI institute, and NASA for supporting its PI institute. Finally, we are indebted to European Space Agency for the tremendous success of MEX, the first ESA mission to the Red Planet.

References

Acuña, M.J., Connerey, J., Ness,N., Lin, R., Mitchell, D., Carlsson, C., McFadden, J., Anderson, K., Rème, H., Mazelle, C., Vignes, D. Wasilewski, P. & Cloutier, P. (1999). Global Distribution of Crustal Magnetization Discovered by Mars Global Surveyor MAG/ER Experiment. *Science* **284**, 790–793.

Barabash, S., P.C. Brandt, O. Norberg, R. Lundin, E.C. Roelof, C.J. Chase, B.H. Mauk, H. Koskinen (1997). Energetic Neutral Atom Imaging by the Astrid Microsatellite, *Adv. Space Res.* **20**, 1055–1060.

Barabash, S., R. Lundin, H. Andersson, M. Holmström & the ASPERA-3 team (2004). ASPERA-3: The Analyser of Space Plasmas and Energetic Atoms for Mars Express, In *Mars Express: The Scientific Payload*, ESA-SP-1240, ESA Publications Division, European Space Agency, Noordwijk, the Netherlands, p.121.

Barabash, S. & the ASPERA-3 team (2004). First Results of the Analyzer of Space Plasma and Energetic Neutral Atoms (ASPERA-3) on Board Mars Express, Invited presentation at the EGU Conference, Nice, France.

Bertaux, J.-L., F. Leblanc, O. Witasse, E. Quemerais, J. Lilensten, S.A. Stern, B. Sandel & O. Koalbev (2005). Discovery of an Aurora on Mars, *Nature* **435**(9), 790–794.

Brain, D.A., Halekas, J.S., Peticolas, L.M., Lin, R.P., Luhmann, J.G., Mitchell, D.L., Delory, G.T., Bougher, S.W., Acuña, M.H. & Rème, H. (2006). On the Origin of Aurorae on Mars, *Geophys. Res. Lett*. DOI: 10.1029/2005GL024782.

Brinkfeld, K., H. Gunell, P.C. Brandt & the ASPERA-3 team (2006). First ENA observations at Mars: Observations of Energetic Neutral Atoms on the Nightside of Mars, *Icarus* **182**(2), 439–447.

Burch, J.L. (2000). IMAGE Mission Overview, *Space Sci. Rev.* **91**, 1–14.

Carlsson, E., A. Fedorov, S. Barabash, R. Frahm, et al. (2006). Mass Composition of the Escaping Plasma at Mars in the Energy Range of 0.6–2 keV, *Icarus* **182**(2), 320–328.

Collier M.R., T.E. Moore, D. Simpson, A. Roberts, A. Szabo, S. Fuselier, P. Wurz, M.A. Lee & B.T. Tsurutani (2004). *Adv. Space Res*. **34**(1), 166–171.

Dubinin, E., R. Lundin , H. Koskinen & N. Pissarenko (1993). Ion Acceleration in the Martian Tail: Phobos Observations, *J. Geophys. Res.* **98**, 3991–3997.

Dubinin, E., D. Winningham, M. Fränz & the ASPERA-3 team (2006). Solar Wind Plasma Protrusion into the Martian Magnetosphere – ASPERA-3 observations, *Icarus* **182**(2).

Espley, J.R., P.A. Cloutier, D.H. Crider, D.A. Brain & M.H. Acuña (2005). Low-frequency Plasma Oscillations at Mars during the October 2003 Solar Storm, *J. Geophys. Res*. **110**, A09S33. DOI: 10.1029/2004JA010935.

Frahm, R., D. Winningham, J. Sharber & the ASPERA-3 team (2006). Carbon Dioxide Photoelectron Peaks at Mars, *Icarus* **182**(2), 371–382.

Futaana, Y., S. Barabash, A. Grigoriev & the ASPERA-3 team (2006a). First ENA Observations at Mars: ENA Emissions from the Martian Upper Atmosphere, *Icarus* **182**(2), 424–430.

Futaana, Y., S. Barabash, A. Grigoriev & the ASPERA-3 team (2006b). First ENA Observations at Mars: Sub-Solar ENA Jet , *Icarus* **182**(2), 413–423.

Futaana, Y., S. Barabash, A. Grigoriev, D. Winningham, R. Frahm & R. Lundin (2006c). Global Response of Martian Plasma Environment to an Interplanetary Shock: From ENA and Plasma Observations at Mars, *Space Sci. Rev*. **126**(1–4), 315–332.

Galli A., P. Wurz, S. Barabash, A. Grigoriev, R. Lundin, Y. Futaana, H. Gunell, M. Holmstöm, E.C. Roelof, C.C. Curtis, K.C. Hsieh, A. Fedorov, D. Winningham, R.A. Frahm, R. Cerulli-Irelli, P. Bochsler, N. Krupp, J. Woch & M. Fraenz (2006). Direct Measurements of Energetic Neutral Hydrogen in the Interplanetary Medium, *Astrophys. J.* **644**(2).

Gringauz, K.I. (1981). A Comparison of the Magnetospheres of Mars, Venus and the Earth, *Adv. Space Res.* **1**, 5–24.

Gruntman, M., Roelof, E.C., Mitchell, D.G., Fahr, H.-J., Funsten, H.O. & McComas, D.J. (2001). Energetic Neutral Atom Imaging of the Heliospheric Boundary Region, *J. Geophys. Res*. **106**, 15767–15782.

Gunell, H., K. Brinkfeldt, M. Holmström & the ASPERA-3 team (2006). Measurements and Simulations of Energetic Neutral Atoms Produced by Charge Exchange at Mars, *Icarus* **182**(2).

Hanson, W.B., Sanatani S. & Zuccaro D.R. (1977). The Martian Ionosphere as Observed by the Viking Retarding Potential Analyzer. *J. Geophys. Res.* **82**, 4351–4363.

Holmström, M., S. Barabash & E. Kallio (2002). Energetic Neutral Atoms at Mars 1. Imaging of Solar Wind Protons, *J. Geophys. Res*. **107**(A10), DOI: 10.1029/2001JA000325.

Holmström M., K. Brinkfeldt, S. Barabash & R. Lundin (2006). Observations in the Shadow of Mars by the Neutral Particle Imager, *Adv. Geosci.*, World Scientific Publications.

Kallio, E. & S. Barabash (2000). On the Elastic and Inelastic Collisions between the Precipitating Energetic Hydrogen Atoms and the Martian Atmospheric Neutrals, *J. Geophys. Res.* **105**(A11), 24973–24996.

Kallio, E. & S. Barabash (2001). Atmospheric Effects of Precipitating Energetic Hydrogen Atoms to the Martian Atmosphere, *J. Geophys. Res*. **106**(1), 165–177.

Kallio, E., J.G. Luhmann & S. Barabash (1997). Charge Exchange near Mars: The Solar Wind Absorbtion and Energetic Neutral Atom Production, *J. Geophys. Res*. **102**, 22183–22197.

Kallio, E., S. Barabash, K. Brinkfeldt & the ASPERA-3 team (2006). Energetic Neutral Atoms (ENA) at Mars: Properties of the Hydrogen Atoms Produced Upstream of the Martian Bow Shock and Implications for ENA Sounding Technique around Non-magnetized Planets, *Icarus* **182**(2), 448–463.

Krymskii, A.M., Breus, T.K., Ness, N.F., Acuña, M.H., Connerney, J.E.P., Crider, D.H., Mitchell, D.L. & Bauer, S.J. (2002). Structure of the Magnetic Field Fluxes Connected with Crustal Magnetization and Topside Ionosphere at Mars. *J. Geophys. Res*. **107**(A9), 1245. DOI: 10.1029/2001JA000239.

Holmström, M., S. Barabash & E. Kallio (2002). Energetic Neutral Atoms at Mars, 1: Imaging of Solar Wind Protons, *J. Geophys. Res.* **107**(A10), 1277. DOI: 10.1029/2001JA000325.

Lallement, R., Qu'emerais, E., Bertaux, J.L., Ferron, S., Koutroumpa, D. & Pellinen, R. (2005). Deflection of the Interstellar Neutral Hydrogen Flow across the Heliospheric Interface, *Science* **307**, 1447–1449.

Lichtenegger, H., H. Lammer & W. Stumptner (2002). Energetic Neutral Atoms at Mars, 3: Flux and Energy Distributions of Planetary Energetic H Atoms, *J. Geophys. Res*. **107**(A10), 1279. DOI: 10.1029/2001JA000322.

Lundin, R., A., Zakharov, R. Pellinen, B. Hultqvist, H. Borg, E.M. Dubinin, S. Barabasj, N. Pissarenkon, H. Koskinen & I. Liede (1989). First Results of the Ionospheric Plasma Escape from Mars, *Nature* **341**, 609–612.

Lundin, R., A. Zakharov, R. Pellinen, S.W. Barabasj, H. Borg, E.M. Dubinin, B. Hultqvist, H. Koskinen, I. Liede & N. Pissarenko (1990). ASPERA/Phobos Measurements of the Ion Outflow from the Martian Ionosphere, *Geophys. Res. Lett*. **17**, 873–876 .

Lundin, R., E. Dubinin, O. Norberg & S. Barabash (1992). Mars Magnetospheric Boundaries and the Acceleration of Ions in the Martian Tail, in *Proc. COSPAR Colloq. 4,* Ann Arbor, MI, USA, pp.311–320.

Lundin, R., S. Barabash, H. Andersson, M. Holmström & the ASPERA-3 team (2004). Solar Wind Induced Atmospheric Erosion at Mars – First Results from ASPERA-3 on Mars Express, *Science* **305**, 1933–1936.

Lundin R., D. Winningham, S. Barabash, R. Frahm, M. Holmström, J.-A. Sauvaud, A. Fedorov, K. Asamura, A.J. Coates, Y. Soobiah, K.C. Hsieh, M. Grande, H. Koskinen, E. Kallio, J. Kozyra, J. Woch, M. Fraenz, D. Brain, J. Luhmann, S. McKenna-Lawler, R. S. Orsini, P. Brandt & P. Wurz (2006a). Plasma Acceleration above Martian Magnetic Anomalies, *Science* **311**, 980–985.

Lundin, R., D. Winningham, S. Barabash & the ASPERA-3 team (2006b). Ionospheric Plasma Acceleration at Mars: ASPERA-3 Results, *Icarus* **182**(2), 308–319.

Mitchell, D.L., Lin, R.P., Mazelle, C. et al. (2001). Probing Mars' Crustal Magnetic Field and Ionosphere with the MGS Electron Reflectometer. *J. Geophys. Res.* **106**, 23419–23428.

Mitchell, D.G., Brandt,, P.C., Roelof, E.C., Dandouras, J., Krimigis, S.M. & Mauk, B.H. (2005). Energetic Neutral Atom Emissions from Titan Interaction with Saturn's Magnetosphere, *Science* **308**, 989–992.

Norberg, O., R. Lundin & S. Barabash (1993). Observation of Molecular Ions in the Martian Plasma Environment, in: Plasma Environments of Non-magnetic Planets (Ed. T.I. Gombosi), *Proc. COSPAR Colloq. 4*, Ann Arbor, MI, USA, pp.299–304.

Roelof, EC., D.G. Mitchell & D.J. Williams (1985). Energetic Neutral Atoms (E≈50 keV) from the Ring Current: IMP7/8 and ISEE 1, *J. Geophys. Res*. **90**, 10991–11008.

Winningham, J.D., R. Frahm, J. Sharber & the ASPERA-3 team (2006). Electron Oscillations in the Induced Martian Magnetosphere, *Icarus* **182**(2), 360–370.

Witte, M. (2004). Kinetic Parameters of Interstellar Neutral Helium: Review of Results Obtained during One Solar Cycle with the Ulysses/GAS-Instrument, *Astron. Astrophys.* **426**, 835–844.

Witte, M., Banaszkiewicz, M., Rosenbauer, H. & McMullin, D. (2004). Kinetic Parameters of Interstellar Neutral Helium: Updated Results from the Ulysses/GAS-instrument, *Adv. Space Res*. **34**, 61–65.